nature portfolio

https://doi.org/10.1038/s41586-026-10412-y

Supplementary information

Engineering tough blood clots for rapid haemostasis and enhanced regeneration

In the format provided by the authors and unedited

Supplementary Materials for

Engineering tough blood clots for rapid hemostasis and enhanced regeneration

Shuaibing Jiang[a], Guangyu Bao[a], Zhen Yang[a], Jing Wu[b], Xingwei Yang[c], Joo Eun (June) Kim[d], Roselyn Jiang[d], Oliver Zhan[a], Alexander Nottegar[a], Yin Liu[b], Zu-hua Gao[e], Andrew Beckett[f], Anastasia Nijnik[d], Rong Long[c], Christian Kastrup[ghi], and Jianyu Li[ab]*

[a] Department of Mechanical Engineering, McGill University, Montreal, Quebec, Canada
[b] Department of Biomedical Engineering, McGill University, Montreal, Quebec, Canada
[c] Department of Mechanical Engineering, University of Colorado Boulder, Boulder, Colorado, USA
[d] Department of Physiology, McGill University, Montreal, Quebec, Canada
[e] Department of Pathology & Laboratory Medicine, University of British Columbia, Vancouver, British Columbia, Canada
[f] Department of Surgery, University of Toronto, Toronto, Ontario, Canada
[g] Michael Smith Laboratories, University of British Columbia, Vancouver, British Columbia, Canada
[h] Versiti Blood Research Institute, Milwaukee, WI, USA
[i] Department of Surgery, Division of Trauma and Acute Care Surgery, and Departments of Biochemistry, Biomedical Engineering, and Pharmacology and Toxicology, Medical College of Wisconsin, Milwaukee, WI, USA

* Corresponding author: jianyu.li@mcgill.ca

Supplementary Figures

Cytogels via cell-crosslinking

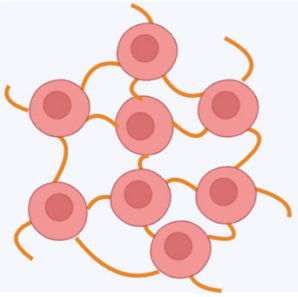

- High cell density
- Fast formation
- Good mechanical properties

Cell aggregate culture

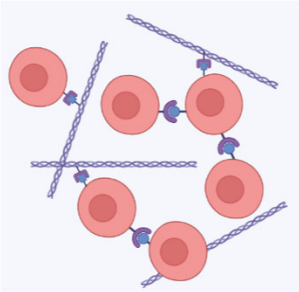

- Slow formation
- Tedious culturing
- Poor mechanical properties

Cell encapsulation

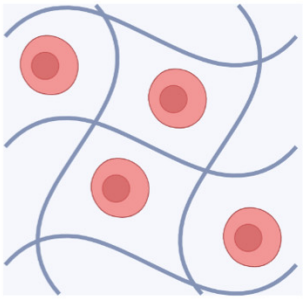

- Low cell density
- Poor cell-cell interaction
- Limited cell activity

Supplementary Scheme 1| Schematic illustrations of approaches to form highly cellularized materials, including cytogels, cell aggregates and cell-laden hydrogels. Figures are created with BioRender.com.

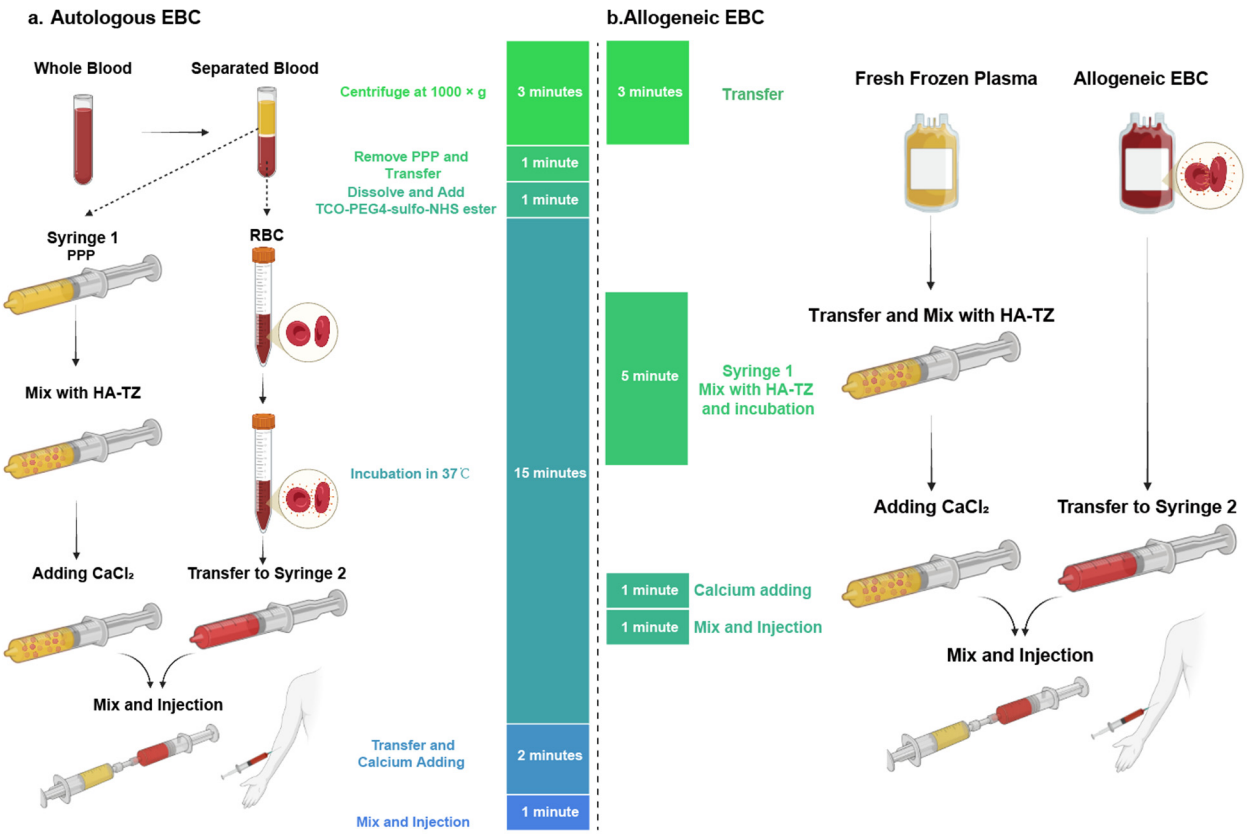

Supplementary Scheme 2| Workflow and timeline for autologous and allogeneic EBCs. Blood can be collected from patients for autologous EBC preparation (**a**). Allogeneic EBCs (**b**) can be prepared from ABO/Rh-matched blood units, starting from pre-modified red blood cells. The indicated timelines are estimates achievable with proper training and routine operation of the EBC preparation procedure. Figures in (**a**, **b**) are created with BioRender.com.

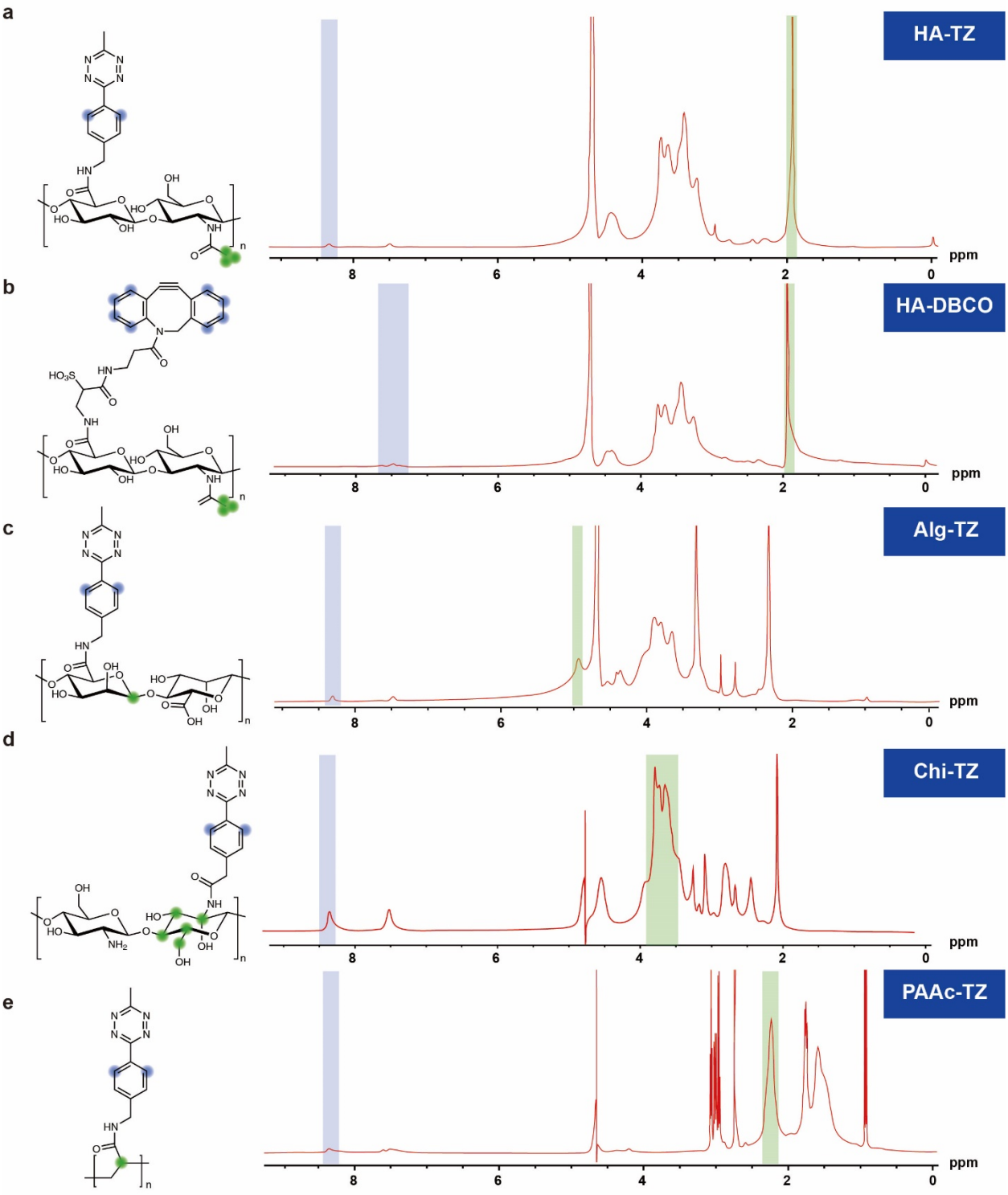

Supplementary Fig. 1| Synthesis and NMR spectra of various polymer linkers. Synthetic schemes and ^{1}H NMR spectra of hyaluronic acid–tetrazine (HA-TZ) prepared via carbodiimide coupling (**a**); hyaluronic acid–dibenzocyclooctyne (HA-DBCO) (**b**); alginate–tetrazine (Alg-TZ) (**c**); chitosan–tetrazine (Chi-TZ) (**d**); and poly(acrylic acid)–tetrazine (PAAc-TZ) (**e**). Blue shading marks protons corresponding to conjugated click-reactive moieties, while green shading marks proton signals from polymer backbones.

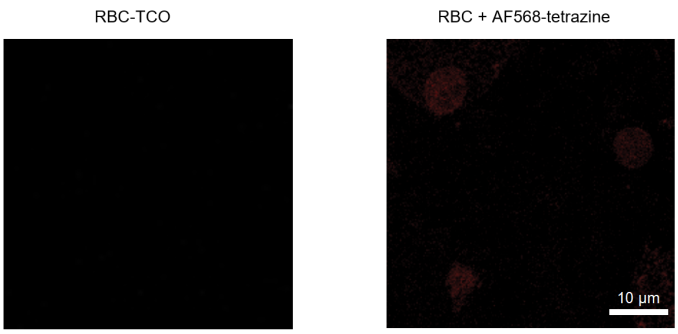

Supplementary Fig. 2| Confocal images of red blood cells (RBC). The modified RBCs (RBC-TCO, left) emit no fluorescence signals, and native RBCs (right) incubated fluorescent dye (AF568-tetrazine) have negligible fluorescence possibly due to non-specific adsorption. Scale bar, 10 μm.

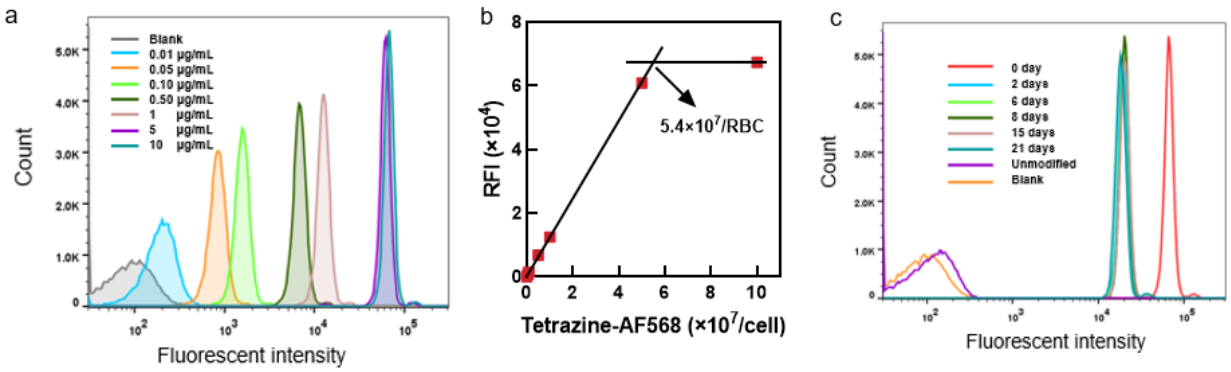

Supplementary Fig. 3| Flow cytometry analysis of modified RBCs. **a**, Measurements of fluorescent intensity from modified RBCs incubated at various concentrations of Tetrazine-AF568. The cell number was kept constant across the groups tested. **b**, Density of TCO on modified RBCs estimated to be 5.4 × 10^7 per cell using titration-based method[46]. **c**, Assessment of TCO stability on modified RBCs over time. Higher fluorescent intensity indicates a greater degree of TCO retention on the RBC surface. The fluorescence maintains stable over 21 days despite an initial decrease.

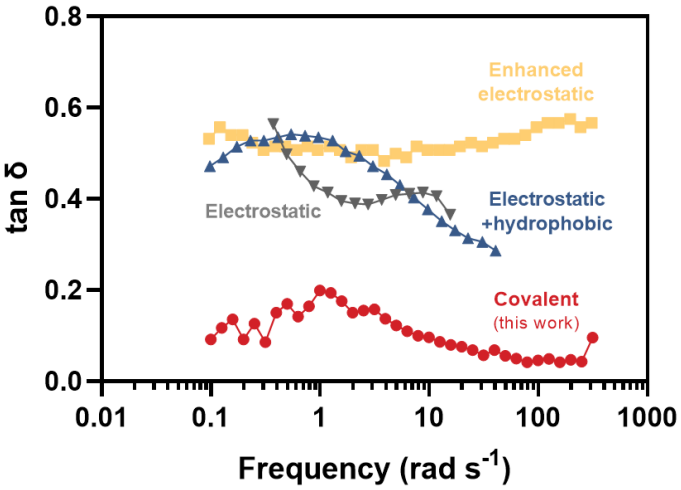

Supplementary Fig. 4| Viscoelastic characteristics of blood gels formed by different strategies. Representative curves of tangent of the phase angle δ (tan δ) of blood gels formed using different strategies. The yellow curve corresponds to blood gels formed with a synthetic polymer comprising cationic and aromatic residues with adjacent sequences. The blue and gray curves represent blood gels formed with hydrophobically modified chitosan and unmodified chitosan, respectively. The RBC cytogels by covalent crosslinking in this work feature small tan δ of around 0.1.

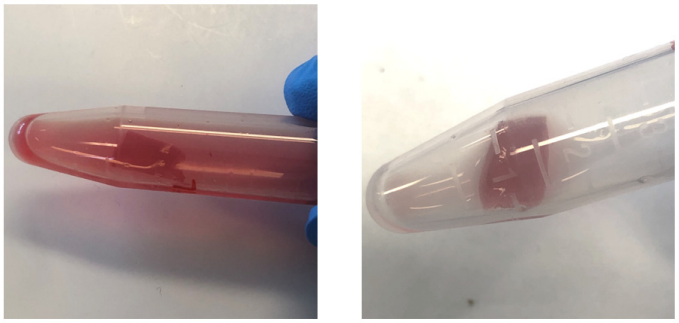

Supplementary Fig. 5| Images of RBC cytogels soaked with DI water. The cells were lysed as shown the released hemoglobin (left), while the RBC cytogels remain intact (right).

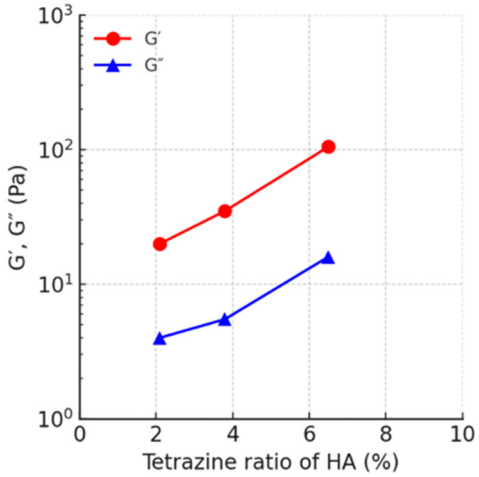

Supplementary Fig. 6| Effect of tetrazine substitution ratio of HA-TZ on shear moduli of RBC cytogels. Storage moduli (G') and loss moduli (G'') of RBC cytogels increase with the tetrazine substitution ratio of HA–TZ, as quantified by ^{1}H NMR spectroscopy, when the RBC volume fraction is fixed at 33% and the HA–TZ concentration is maintained at 1 wt%.

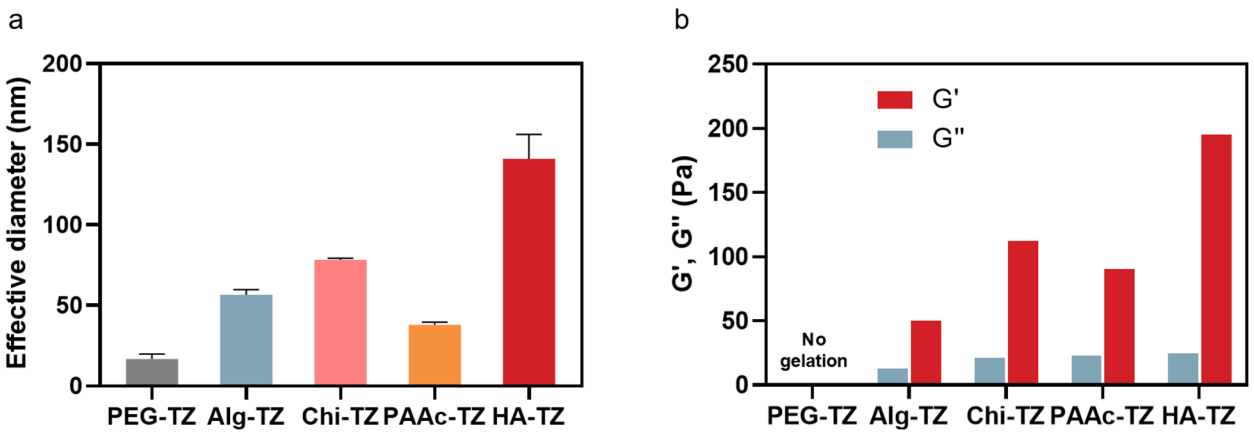

Supplementary Fig. 7| Characterization of polymer linkers and the resulting RBC cytogels. **a**, Hydrodynamic diameters of various polymer linkers measured using dynamic light scattering. PEG, Alg, Chi, PAAc and HA denote polyethylene glycol, alginate, chitosan, polyacrylic acid and hyaluronic acid, respectively. Data are presented as mean ± SD (n = 3). **b**, Shear moduli of the RBC cytogels formed using different polymer linkers.

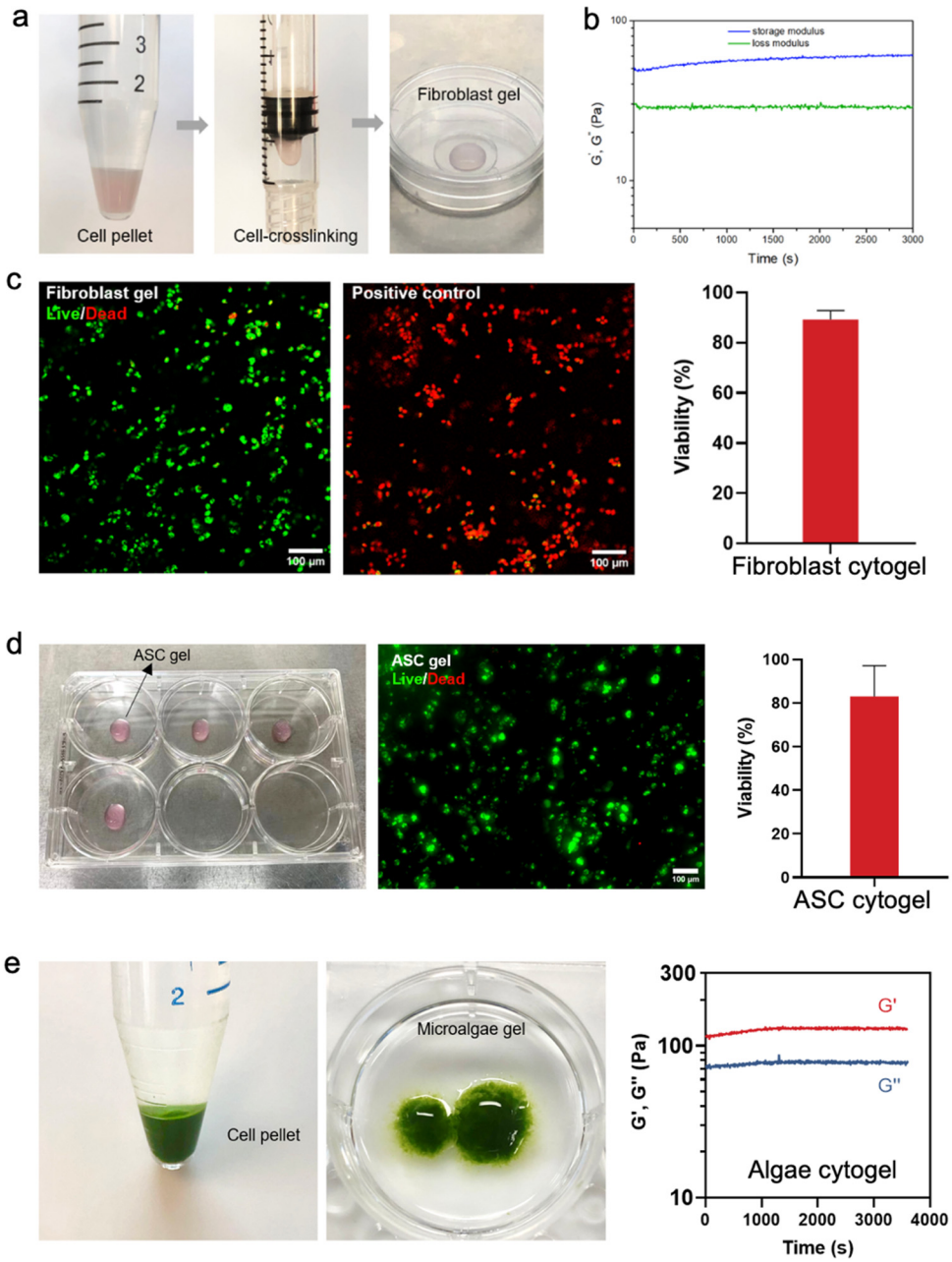

Supplementary Fig. 8| Gelation and cytocompatibility of various cytogels. (a–c) Fibroblast cytogels. **a**, Digital images showing the formation of fibroblast cytogels with high cell density (~5 × 10^7 cells/mL) through direct crosslinking of human vocal fold fibroblasts (hVFFs). **b**, Rheological analysis demonstrating immediate gelation upon mixing modified hVFFs with the polymer linker, yielding a storage modulus of 60 Pa and a loss modulus of 30 Pa. **c**, LIVE/DEAD staining of cells within fibroblast cytogels, where live cells are stained green and dead cells red. Cytogels treated with 70% ethanol serve as a positive control for dead cell staining. Viability analysis shows 89% live hVFFs. Data are presented as mean ± SD (n = 5). **d**, Adipose-derived stem cell (ASC) cytogels. Digital images showing living ASC gels with high cell density (~4 × 10^6 cells/mL) formed via cell crosslinking in a tissue culture plate. LIVE/DEAD staining indicates high cell viability, with live cells in green and dead cells in red. ASC viability within the cytogels is 83%. Data are presented as mean ± SD (n = 3). **e**, Microalgae cytogels. Image of microalgae cell pellet after centrifugation and digital photo showing formation of living microalgae cytogels with high cell content (~33% by volume). Rheological analysis confirms rapid gelation via the click-clotting strategy, achieving a storage modulus of 120 Pa and a loss modulus of 70 Pa.

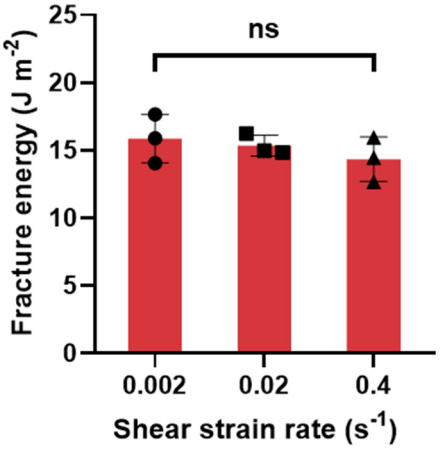

Supplementary Fig. 9| Effect of shear strain rate on the fracture energy of RBC cytogels. Data are presented as mean ± SD (n = 3). Statistical significance and *P* values were determined by one-way ANOVA with post hoc Tukey tests. The “ns” denotes no significant difference.

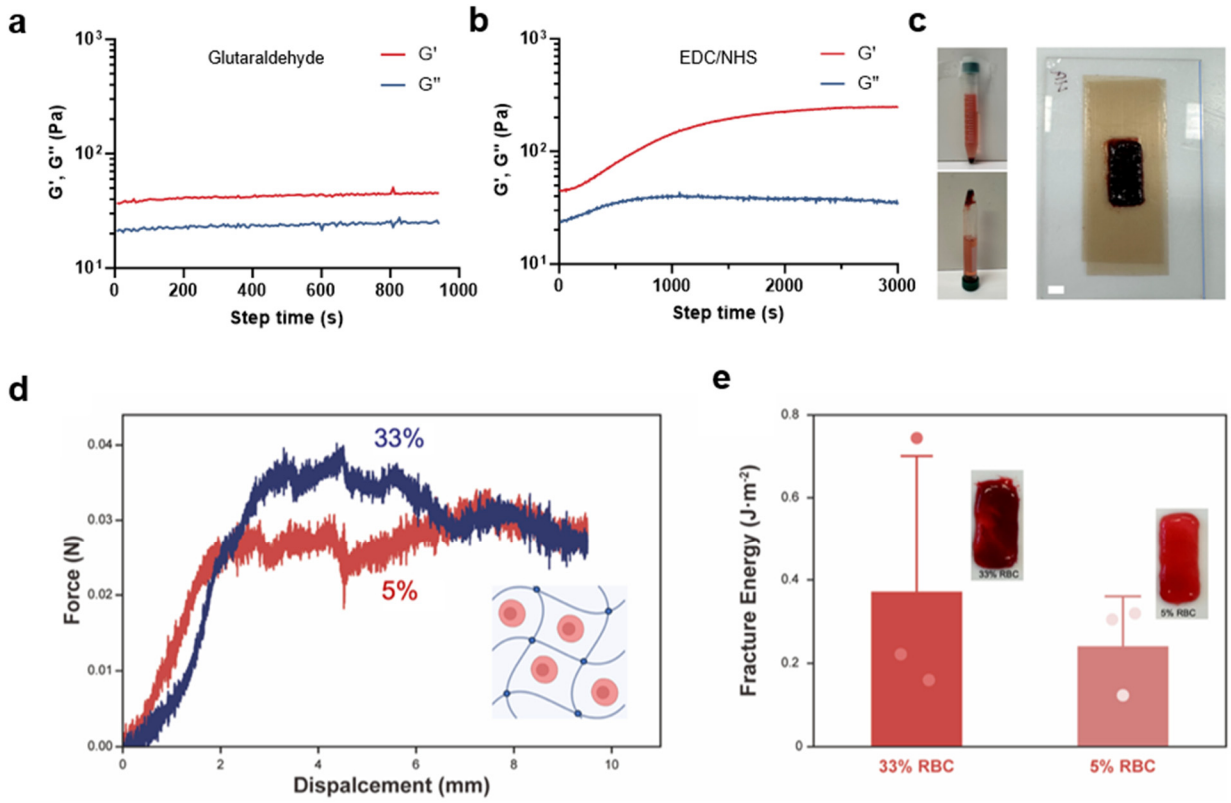

Supplementary Fig. 10| Mechanical characterization of control clots. a, Time-sweep test of RBC–HA mixtures crosslinked with glutaraldehyde. G' and G'' denote storage (red) and loss (blue) modulus, respectively. **b**, Time-sweep test of RBC–HA mixtures crosslinked with EDC and NHS. **c**, Images of EDC/NHS-crosslinked clots, showing substantial RBC lysis and poor gel integrity, as evidenced by the inability of the gel to support its own weight upon vial inversion. The resulting EDC/NHS-crosslinked clot deposited in a mold. Scale bar, 5 mm. **d**, Representative force–displacement curves from modified lap-shear tests of RBC-encapsulated click HA hydrogels; inset, schematic of the click-crosslinked HA network containing unmodified RBCs. **e**, Fracture energy of RBC-encapsulated click HA hydrogels, demonstrating significantly lower toughness compared to EBCs. Sample size: n = 3. Data are presented as mean ± SD.

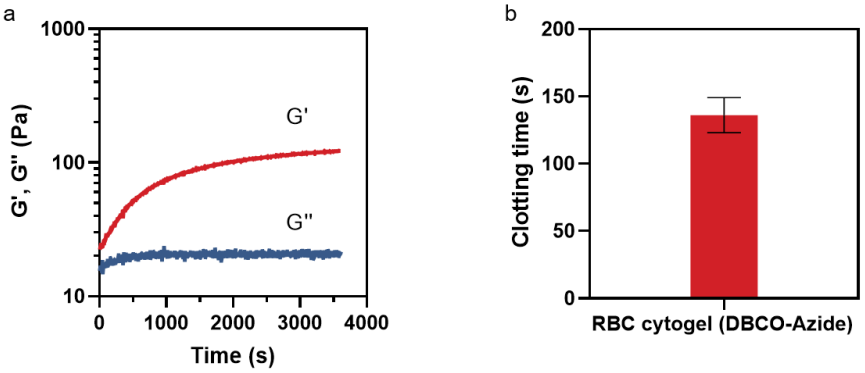

Supplementary Fig. 11| Clotting kinetics of RBC cytogel using DBCO-Azide ligation. **a**, Representative clotting profiles of RBC cytogel using DBCO-Azide ligation, measured by rheology. **b**, Clotting time of RBC cytogel (DBCO-Azide) was determined by the inverted vial test. Due to the viscous nature of the mixture, although the initial G′ is higher than G″ as shown in the rheology, the mixture is still flowable. Thus, we used the inverted vial test to measure the clotting time. Data are presented as mean ± SD (n = 3).

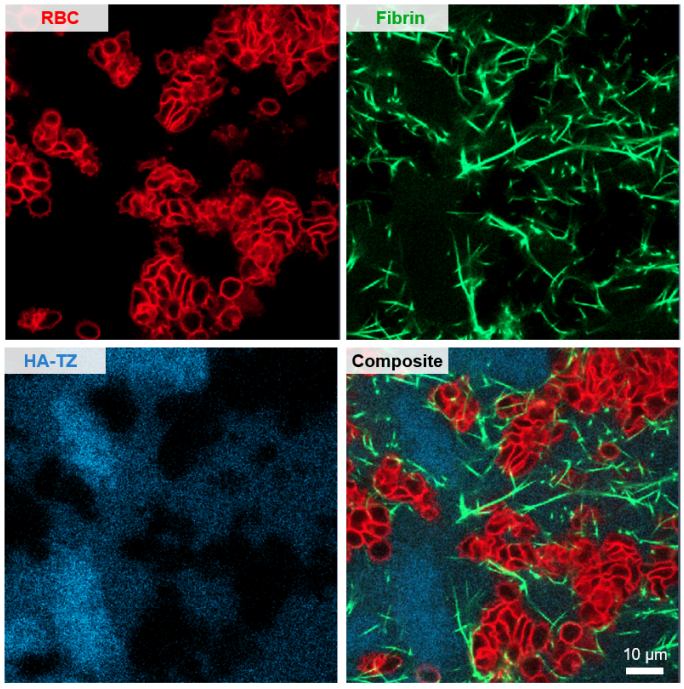

Supplementary Fig. 12| Confocal images of control blood clots formed with unmodified RBCs. They consist of unmodified RBCs (red), HA-TZ (blue) and fibrin (green). The unmodified RBCs fail to form a continuous network and are instead encapsulated within the fibrin matrix as discrete clusters.

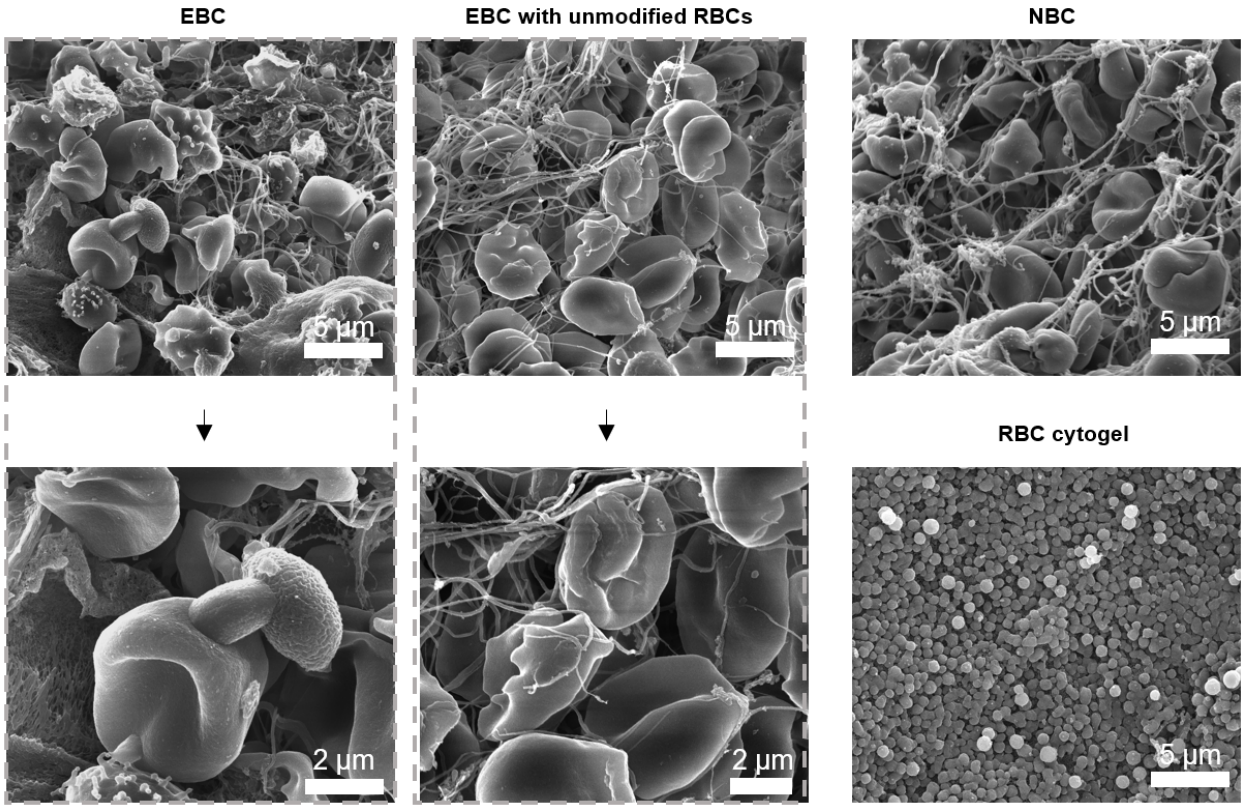

Supplementary Fig. 13| SEM images of EBC with and without modified RBCs, compared to NBC and RBC gels. The modified RBCs within EBC are linked together, forming a cohesive structure (left column), while unmodified RBCs in the control (middle column) or NBC are either separated or trapped in the fibrin network. The cells within the RBC cytogels appear smaller in size due to the dehydration process during SEM sample preparation.

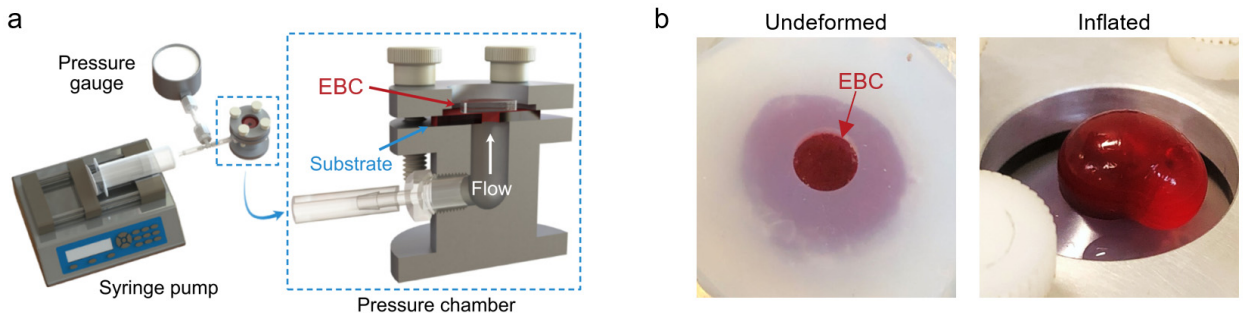

Supplementary Fig. 14| Burst pressure test. **a**, Schematic illustration of the setup used to measure burst pressure. **b**, Images of undeformed EBC under no pressure (left) and highly deformed EBC, sustaining high pressure before burst (right).

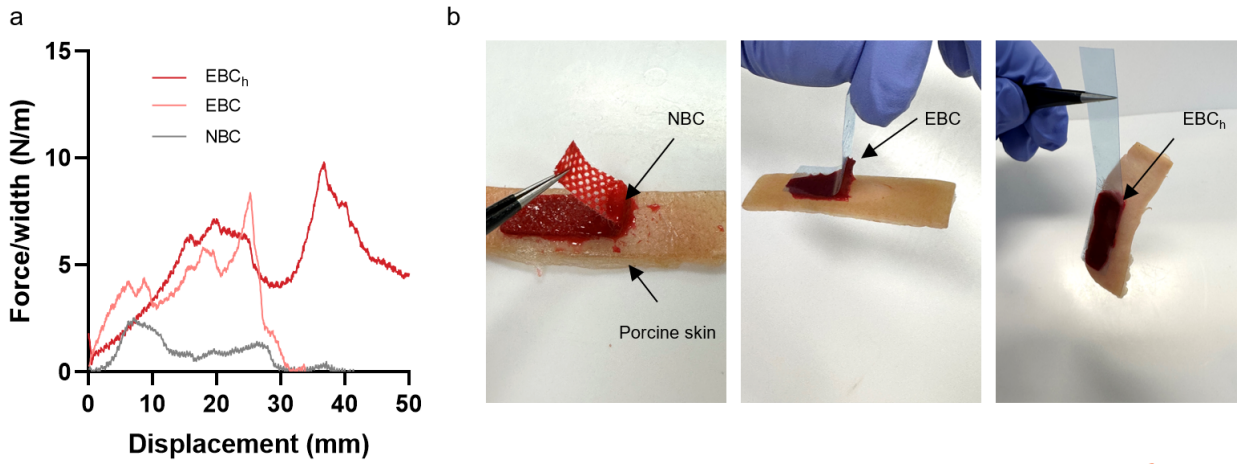

Supplementary Fig. 15| Peeling test. **a**, Representative force-displacement curves of EBC and NBC under 180-degree peeling test. The curves were smoothed (second order smoothing,15 neighbors). **b**. Images of NBC, EBC and EBC_h (containing physiological fibrin content) adhered on porcine skin. The adhesion of NBC cannot sustain the skin during lifting, while the EBC and EBC_h lift the skin firmly.

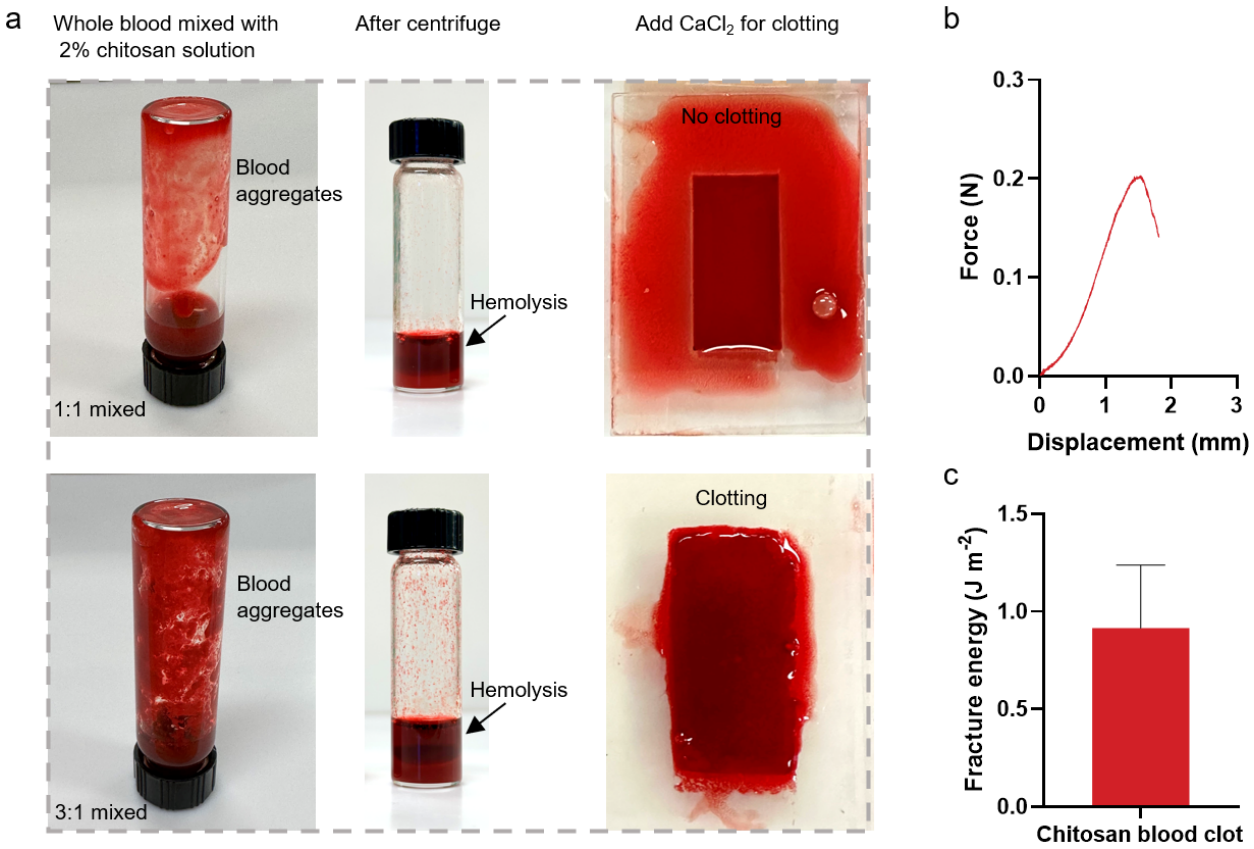

Supplementary Fig. 16| Synthesis and characterization of blood/chitosan aggregates. **a**, No self-supporting gel is formed upon mixing human whole blood with 2% chitosan solution at varied ratios (blood:chitosan = 1:1 or 3:1) (left). Aggregates are formed due to electrostatic interactions between blood cells and chitosan, but significant hemolysis occurs as well (middle). Too much chitosan impairs blood clotting with the addition of $CaCl_2$, which is possibly because the chitosan solution changes the pH of whole blood (right). **b, c**, Representative force-displacement curve (**b**) and the calculated fracture energy (**c**) of whole blood/chitosan (3:1) clots under lap-shear test. Data are presented as mean ± SD (n = 3).

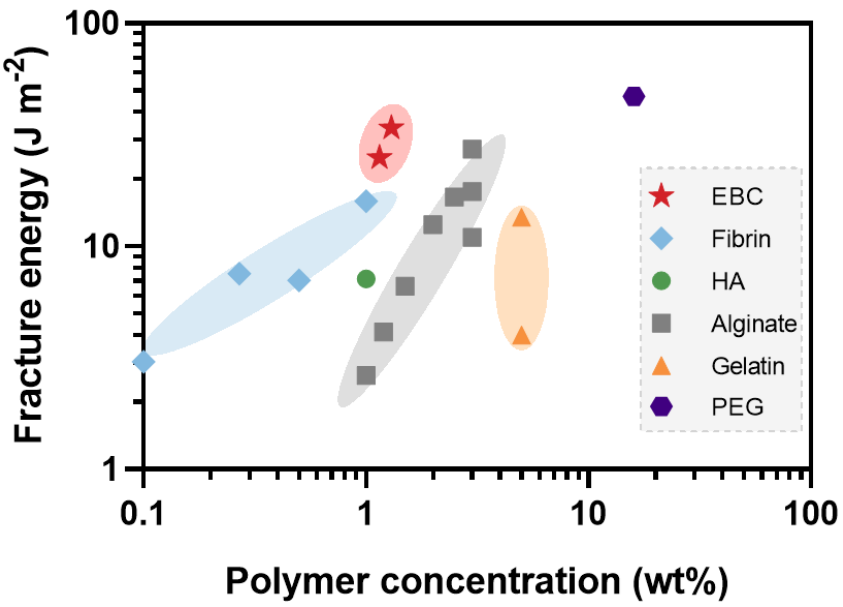

Supplementary Fig. 17| Fracture energy of EBC and other polymeric hydrogels at varied polymer concentration. EBC are significantly tougher than other hydrogels at the same polymer concentration. Data were collected from previous reports on fibrin[56], alginate[21,57], gelatin[58,59] and PEG hydrogels[60]. The fracture energy of HA hydrogel was tested with the same method in this study using the covalently crosslinked hydrogel formed by HA-TZ and HA-NB (norbornene).

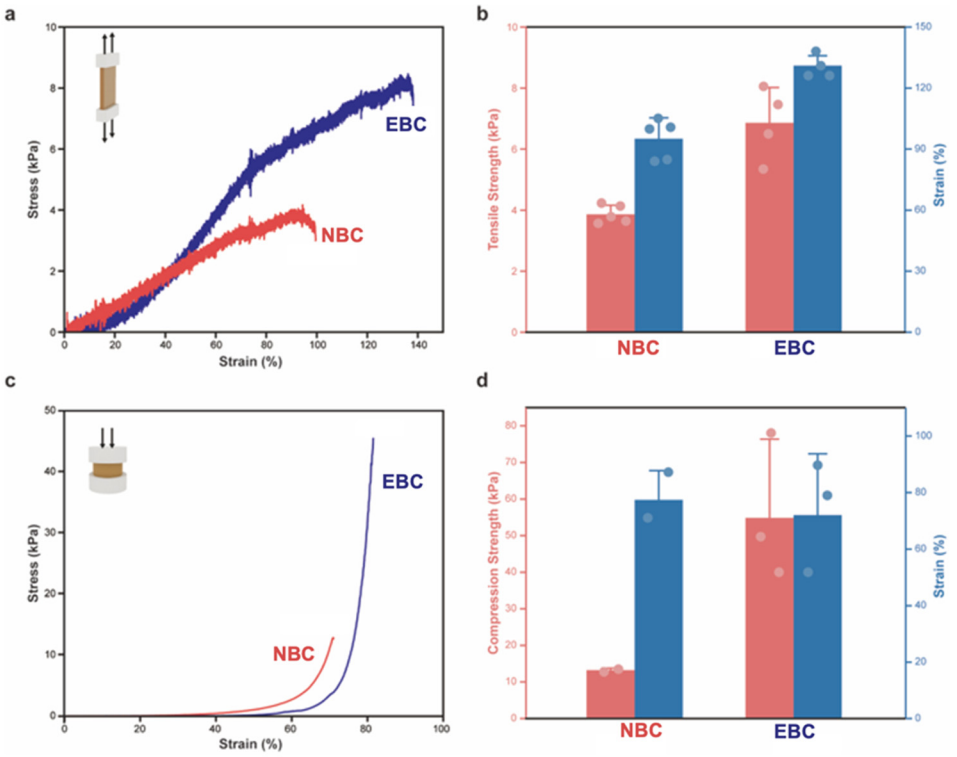

Supplementary Fig. 18| Tensile and compressive tests. a, Stress-strain curves under tension. **b**, Tensile strength and maximum tensile strain. **c**, Stress-strain curves under compression. **d**, Compressive strength and maxim compressive strain. Data are presented as mean ± SD.

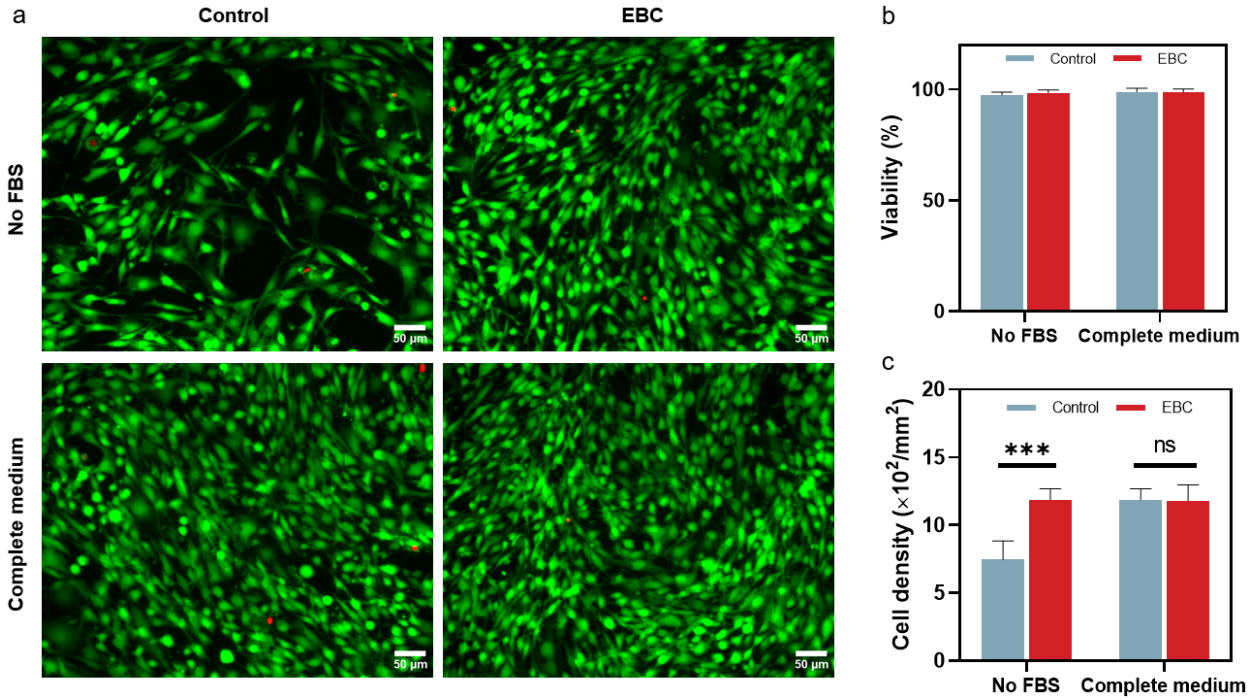

Supplementary Fig. 19| Cytocompatibility test using *in vitro* culture of human vocal fold fibroblasts (hVFFs). a, Representative images of hVFFs cultured with extract of EBC, both with and without the supplement of fetal bovine serum (FBS) in the medium. Living cells were stained in green, while dead cells were stained in red. Cells cultured on a 96-well plate as the control. **b**, Viability analysis indicates that cells in all groups exhibit a viability of approximately 100%. **c**, Cell density in the EBC group is significantly higher than that in the control when no FBS added to the media. Data are presented as mean ± SD (n = 10). Statistical significance and *P* values were determined by two-sided t-test for the comparison between two groups. ****P* < 0.001, ns denotes no significant difference.

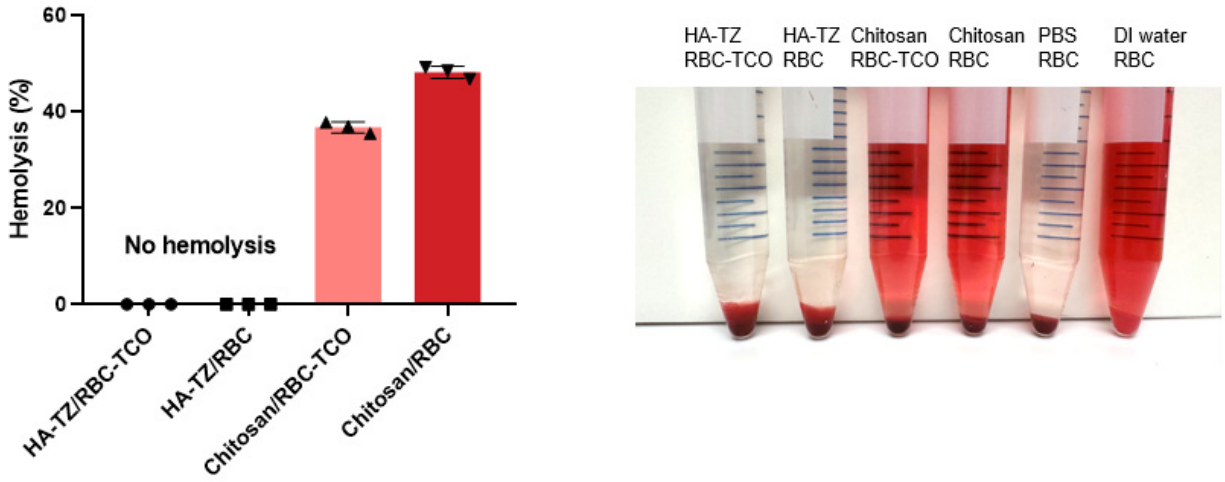

Supplementary Fig. 20| **Hemolysis test**. Comparison of hemolysis of pristine and modified RBC resulted by bioorthogonal polymer linkers and other materials, including chitosan, PBS and DI water. No hemolysis is found with polymer linkers, while chitosan causes significant hemolysis. Data are presented as mean ± SD (n = 3).

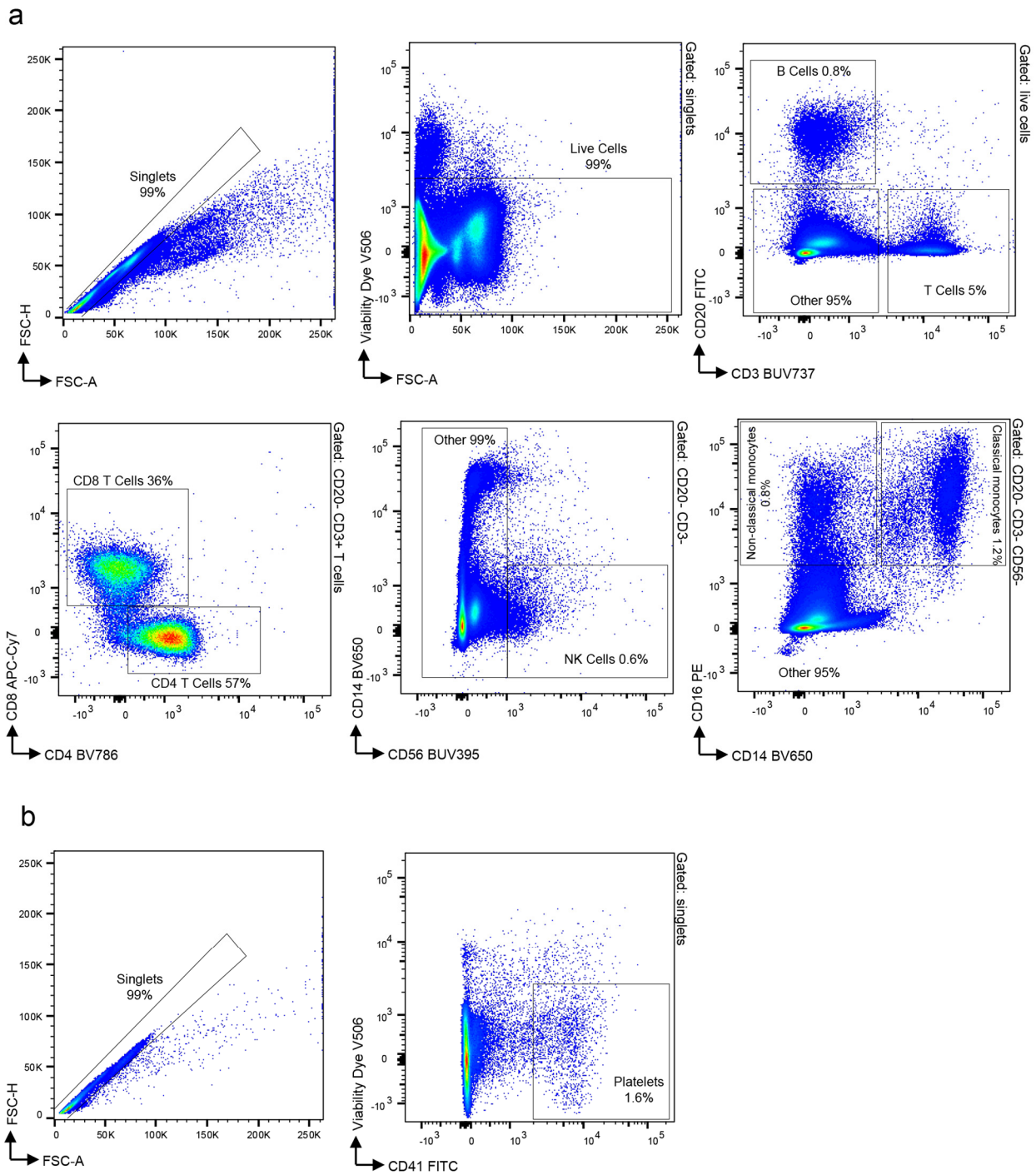

Supplementary Fig. 21| Flow cytometry gating strategies for the peripheral blood mononuclear cell samples, showing the gating on single live cells, followed by (**a**) gating of CD4 T cells as CD3+CD4+CD20-, CD8 T cells as CD3+CD8a+CD20- cells, B cells as CD20+CD3- cells, NK cells as CD3-CD20-CD56+ cells, classical monocytes as CD3-CD20-CD56-CD14+, non-classical monocytes as CD3-CD20-CD56-CD14-CD16+, and (**b**) platelets based on CD41+. The percentage of cells within each gate relative to the parent gate is indicated.

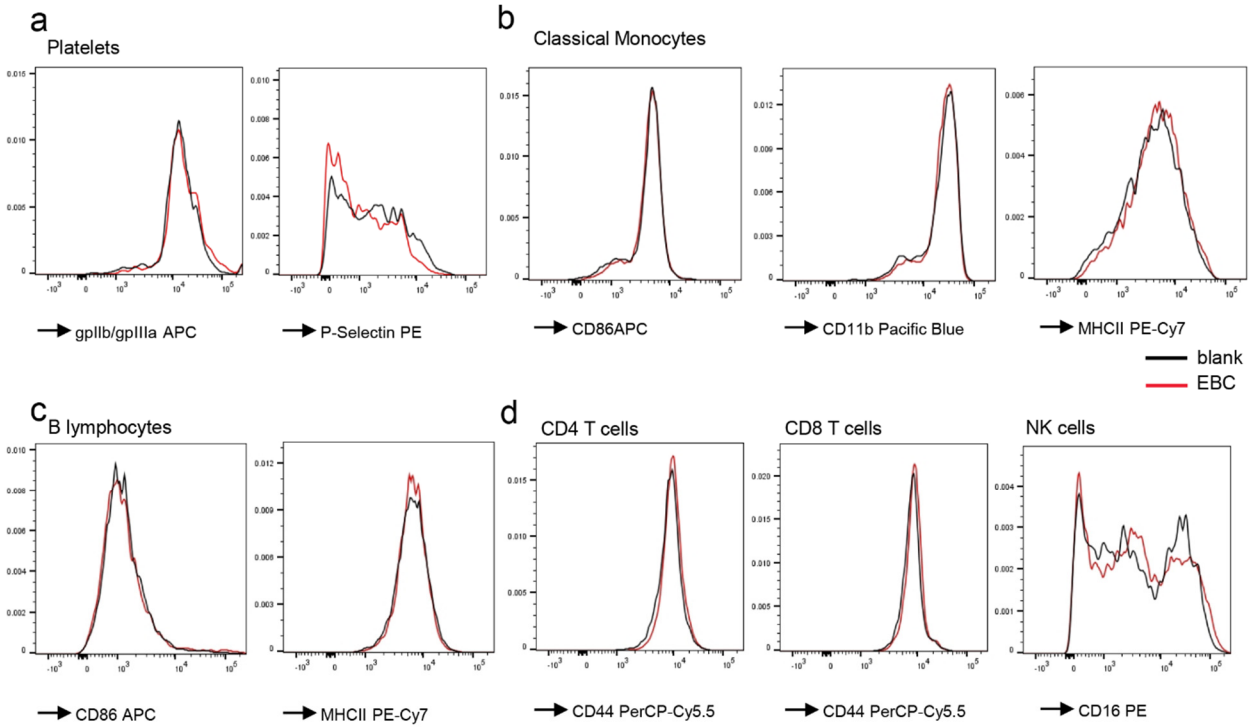

Supplementary Fig. 22| Representative flow cytometry histograms showing the expression of activation markers on (**a**) platelets, (**b**) classical monocytes, (**c**) B lymphocytes, (**d**) T cells and NK cells, comparing the control peripheral blood cell samples (black) with blood pre-incubated with EBC (red) for each cell type and marker.

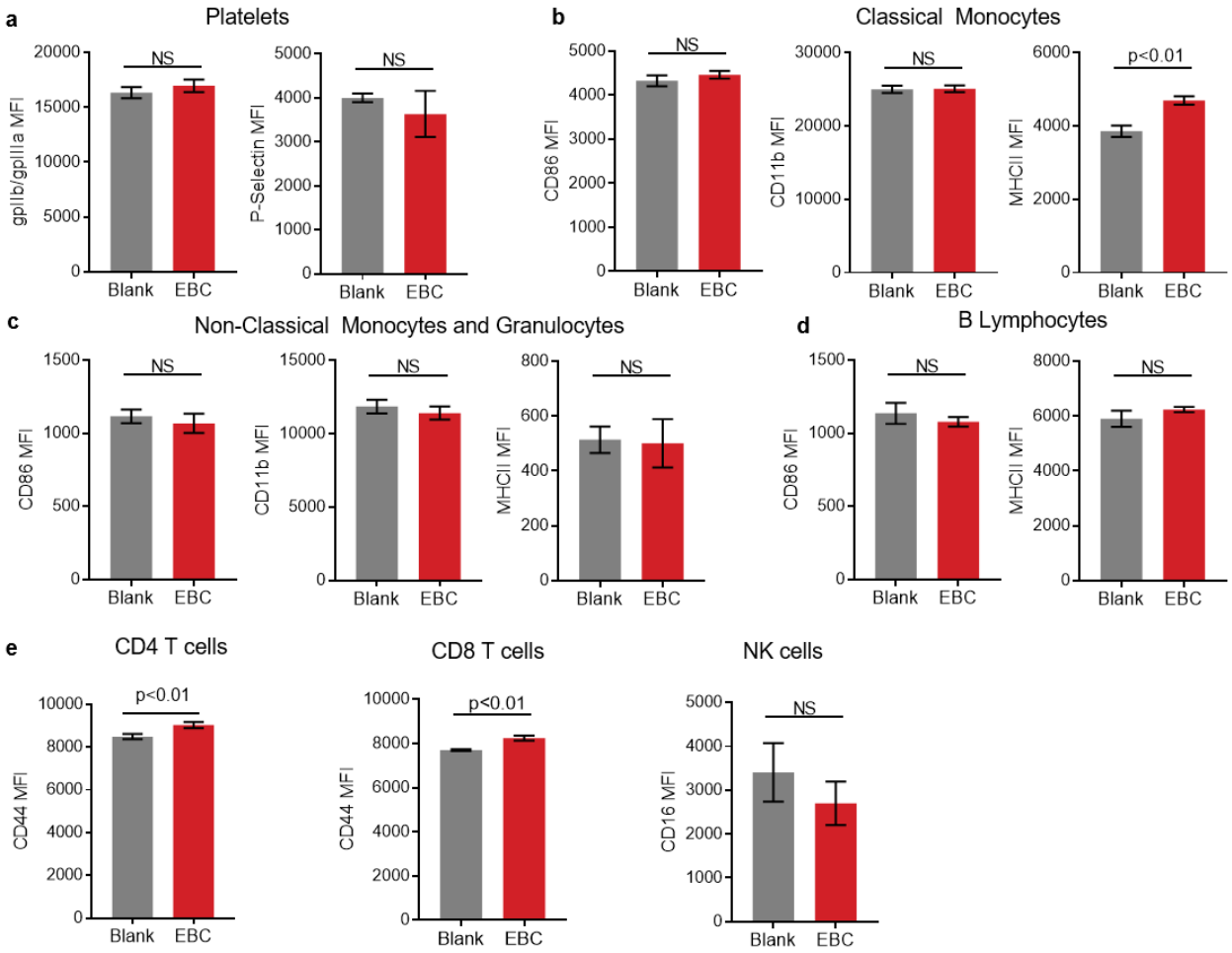

Supplementary Fig. 23| Blood cell compatibility of EBC. Normal anticoagulated human whole blood was incubated with EBC. The incubated blood cells were then separated and analyzed using flow cytometry to assess the responses of various cell types, including platelets (**a**), monocytes (**b**), granulocytes (**c**), B lymphocytes (**d**), T cells and Natural Killer (NK) cells (**e**). The expression of activation markers on each cell type is presented as mean fluorescence intensity (MFI). Data are presented as mean ± SD (n = 3). Statistical significance and *P* values were determined by Student's unpaired t-test for the comparison between two groups. NS denotes no significant difference.

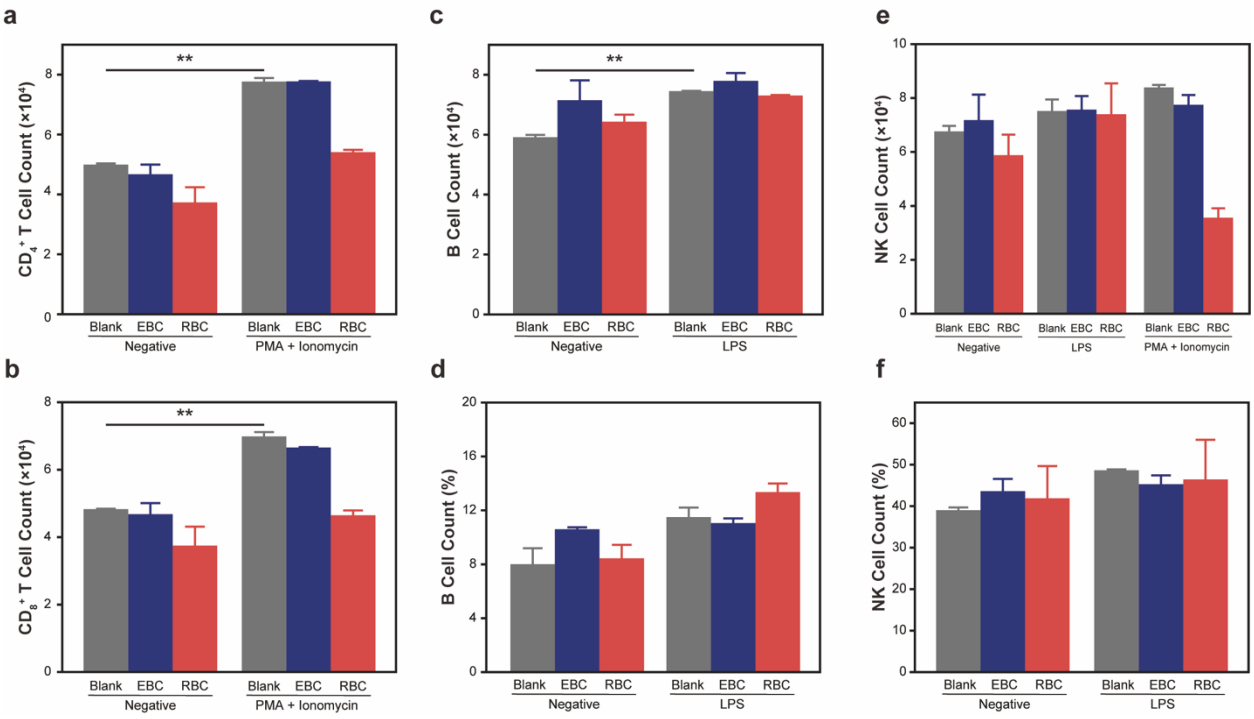

Supplementary Fig. 24| Immune profiling of allogeneic EBCs in freshly isolated human blood. Flow-cytometry analysis comparing peripheral blood mononuclear cells (PBMCs) from blank (non-treatment), EBC-treated, and unmodified RBC-treated conditions. Lipopolysaccharide (LPS) and phorbol 12-myristate 13-acetate (PMA) plus ionomycin were used as positive controls to confirm preserved immune responsiveness. Quantification of (**a**) $CD4^+$ T cell counts, (**b**) $CD8^+$ T cell counts, (**c**) B cell counts ($HLA\text{-}DR^+$, $CD86^+$), (**d**) B cell percentage, and (**e**) natural killer (NK)-cell counts ($CD44^+$, $CD16^+$) with (**f**) NK-cell percentage. No significant activation or expansion of lymphocyte subsets was observed in the EBC-treated group relative to blank controls. Data are presented as mean ± SD. Statistical analysis was performed using two-sample unpaired t-tests.

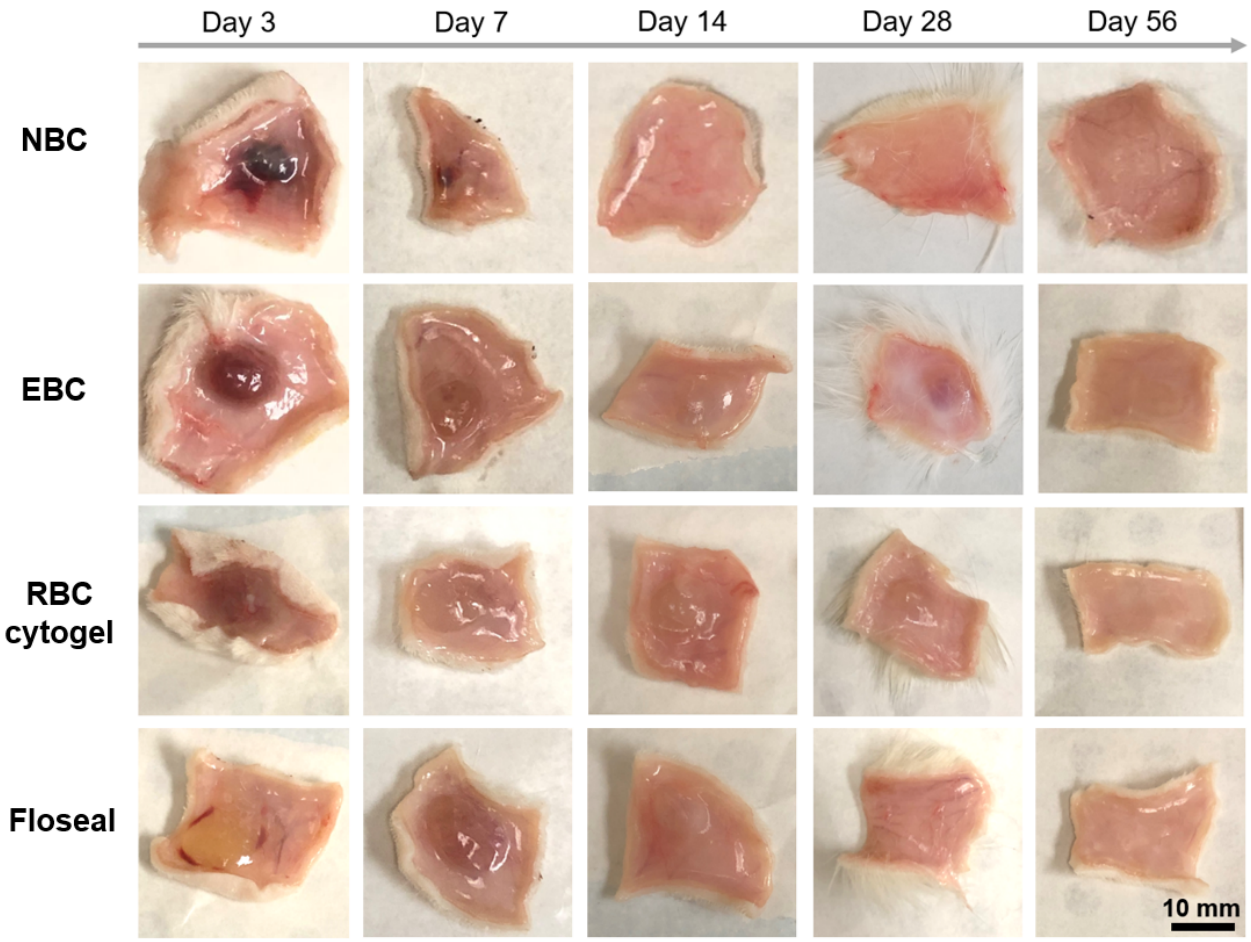

Supplementary Fig. 25| Biodegradation comparison of EBC with NBC, RBC cytogels and Floseal. Photos of the implants and adjacent tissues harvested at various time points from a rat subcutaneous implantation model. Scale bar, 10 mm.

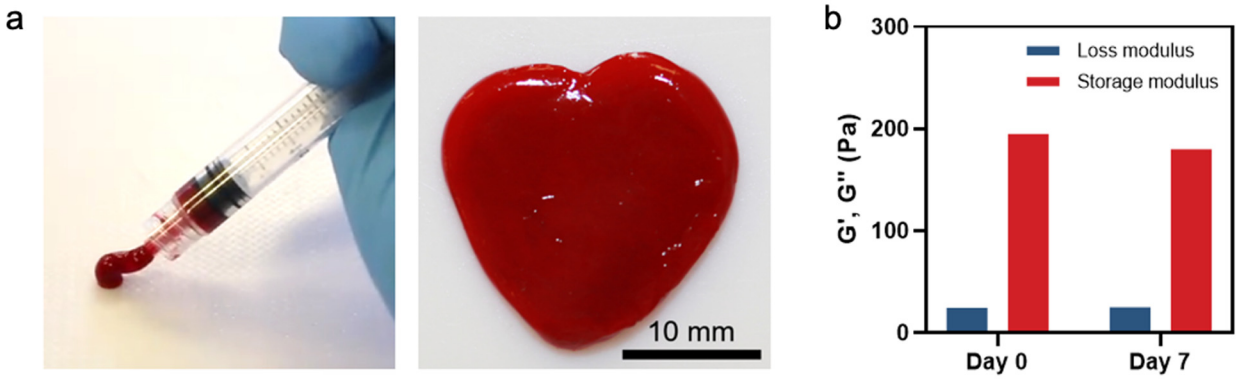

Supplementary Fig. 26| **Injectability and storage stability of EBC**. **a**. EBC is injectable through syringe and can maintain its shape. **b**. Shear moduli of RBC cytogel prepared using modified RBCs as prepared or after 7-day storage at 4°C.

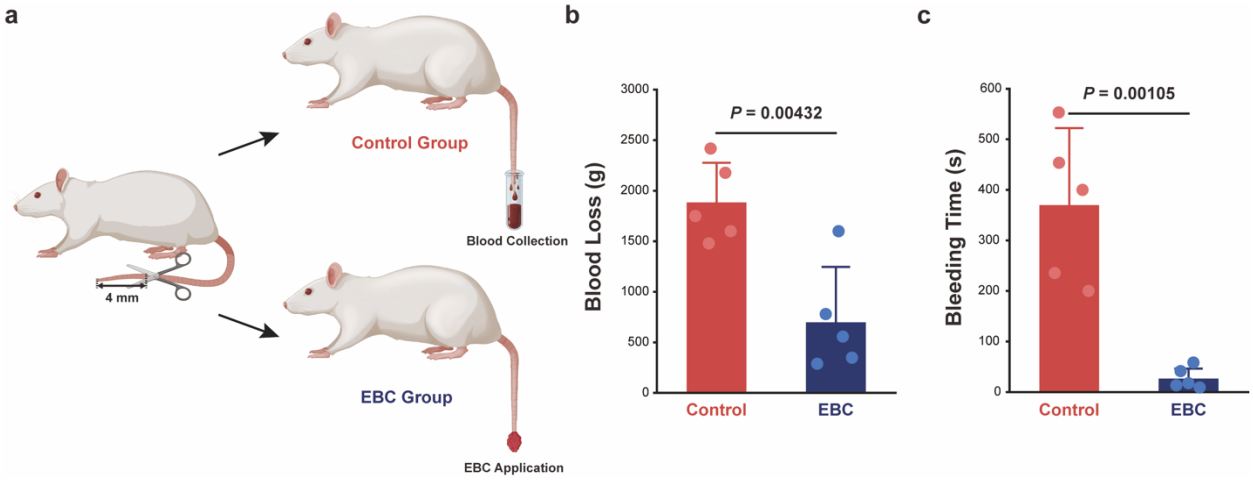

Supplementary Fig. 27| Rat tail amputation model. (a) Schematic illustration of the experimental setup showing the non-treated control group and the EBC-treated group, where EBC was prepared from the blood of one rat and applied to another. (b) Quantification of total blood loss. (c) Measurement of bleeding time. Sample size: n = 5 per group; data are presented as mean ± SD. Figures in **a** are created with BioRender.com.

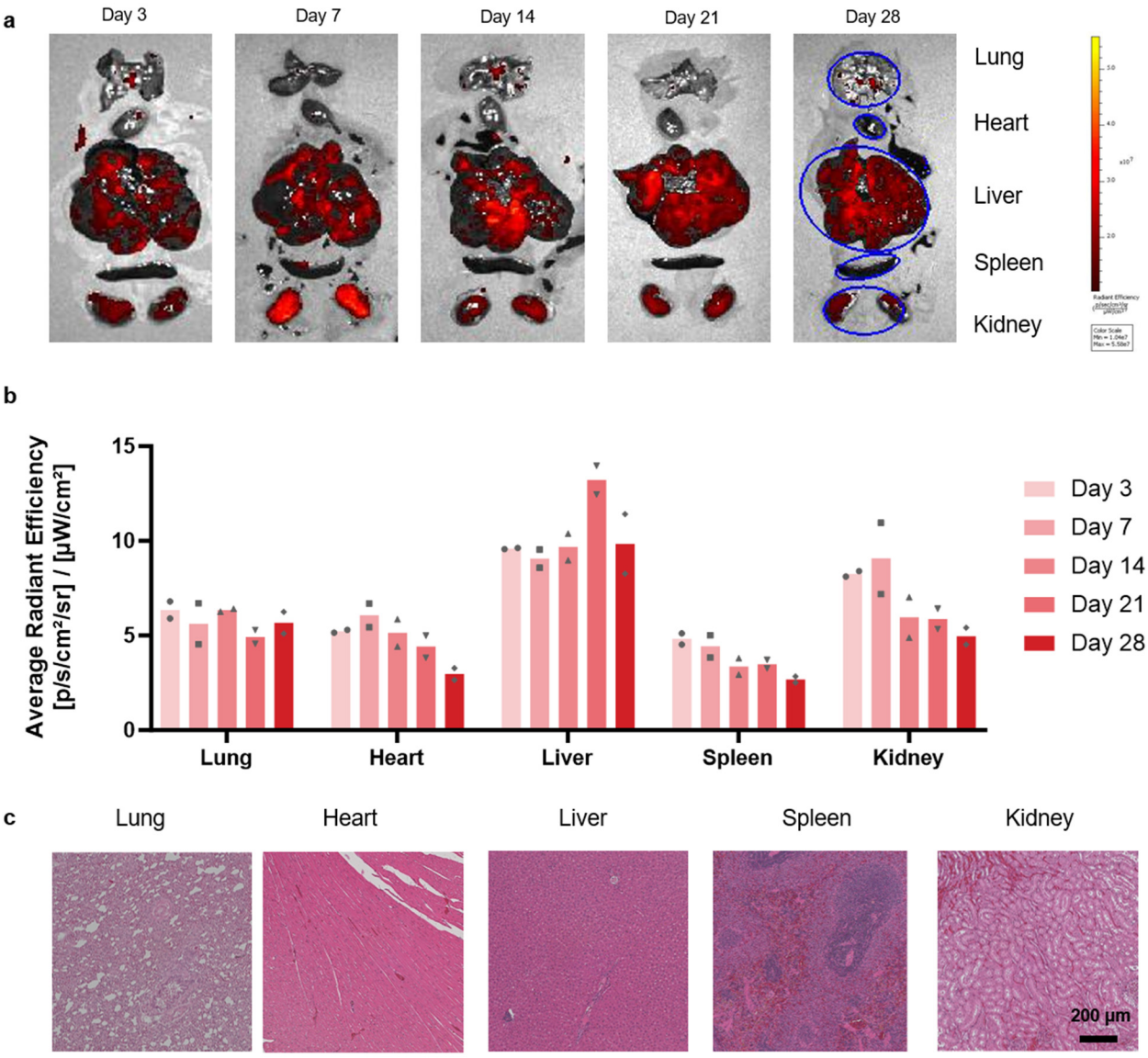

Supplementary Fig. 28| Biodistribution and systemic toxicity of EBC. a, Biodistribution of degraded products from EBC containing FITC-labelled HA in major organs over a 28-day period of subcutaneous implantation. b, Average fluorescent intensity of major organs over time. Individual data points are shown; vertical bars indicate the mean (n = 2). c, Histological sectioning (H&E) showing no toxicity of the degraded byproducts to major organs.

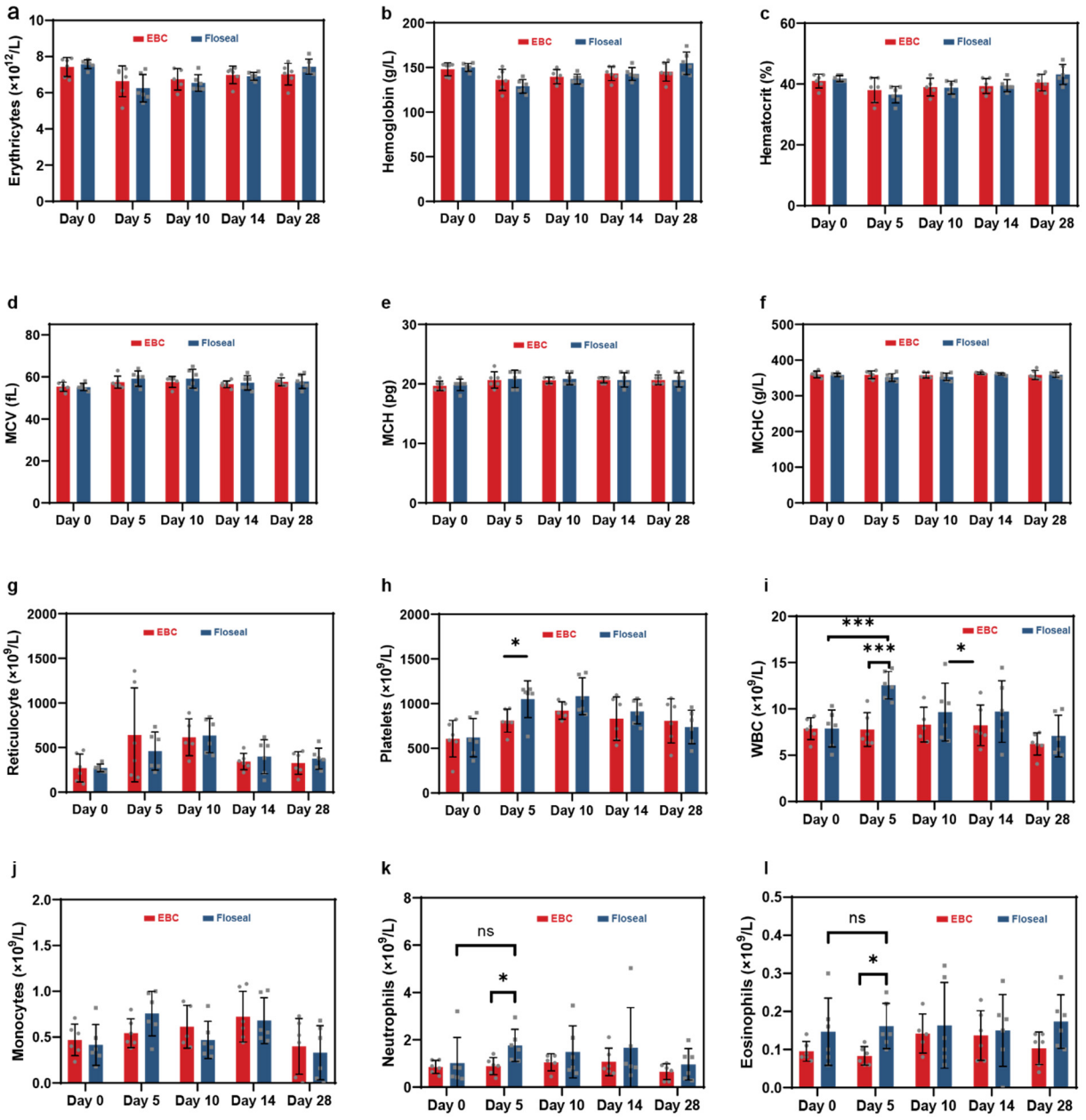

Supplementary Fig. 29| Hematology test of complete blood counting over 28 days of implantation. **a**, Erythrocytes. **b**, Hemoglobin. **c**, Hematocrit. **d**, Mean corpuscular volume (MCV). **e**, Mean corpuscular hemoglobin (MCH). **f**, Mean corpuscular hemoglobin concentration (MCHC). **g**, Reticulocytes. **h**, Platelets. **i**, White blood cells (WBC). **j**, Monocytes. **k**, Neutrophils. **l**, Eosinophils. Data are presented as mean ± SD (n = 6). 0.01 < *P < 0.05, ***P < 0.001, ns denotes no significant difference.

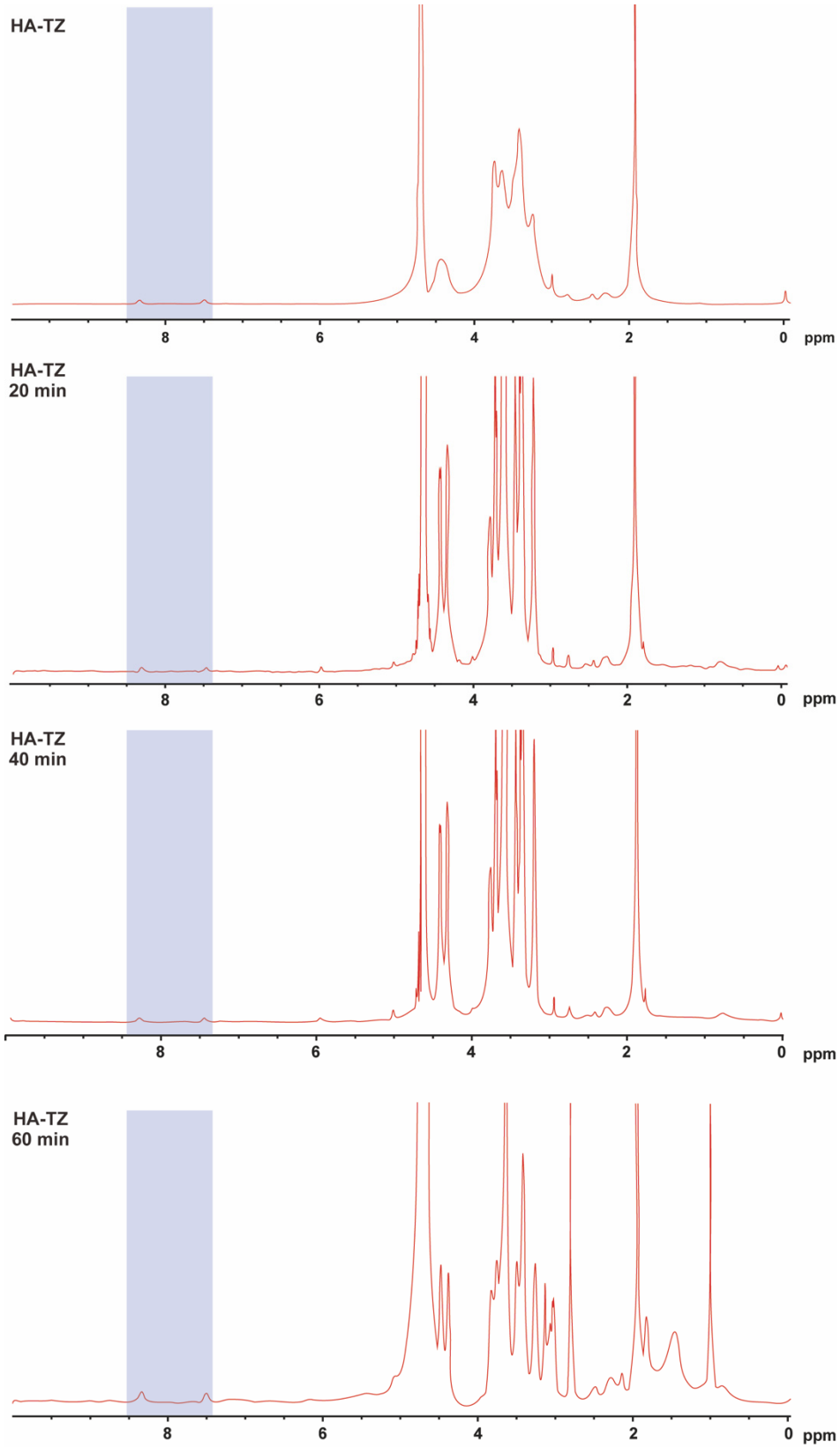

Supplementary Fig. 30| ^{1}H NMR spectra of HA-TZ with varying molecular weights produced by hyaluronidase digestion for 20, 40, and 60 minutes.

Supplementary Tables

Supplementary Table 1| Degree of substitution of tetrazine calculated from ^{1}H NMR.

HA polymers	EDC/NHS	Tetrazine feed ratio	Nominal ratio	Ratio from ^{1}H NMR	Tetrazine per HA chain*
HA-TZ10	2.5–fold of -COOH	0.25 mmol/g	10%	~2.1%	~130
HA-TZ20	2.5–fold of -COOH	0.5 mmol/g	20%	~3.8%	~238
HA-TZ	2.5–fold of -COOH	0.75 mmol/g	30%	~6.5%	~407

*Calculated based on the molecular weight of HA (~2380 kDa) as measured by gel permeation chromatography.

Supplementary Table 2| Molecular weights and hydrodynamic sizes of HA–TZ polymers*

Sample	Hyaluronidase reaction (min)	M_w (g/mol)	M_n (g/mol)	PDI	Hydrodynamic size (nm)
HA-TZ	0	2381621	1263259	1.89	144.5
HA20-TZ	20	581784	297869	1.95	52.9
HA40-TZ	40	365293	176445	2.07	32.8
HA60-TZ	60	256719	132254	1.94	21.6

* M_n, number-average molecular weight; M_w, weight-average molecular weight; PDI = M_w/M_n, polydispersity index indicating the breadth of the molecular weight distribution.

Supplementary Table 3| Comparison between EBC and other biomaterials for liver regeneration.

Biomaterials	Animal models	Wound size	Inflammation	Foreign body responses?	Liver regeneration
EBC (this work)	Rat liver volumetric injury	4 mm in diameter and 3 mm in depth	Very mild	Minimal	Day 5: 78% Day 14: 82% Day 28: ~100%
Floseal (this work)	Rat liver volumetric injury	4 mm in diameter and 3 mm in depth	Moderate ~ severe	Yes	Day 5: 20% Day 14: 51% Day 28: 84%
Barnacle-glue-inspired paste[5]	Rat liver volumetric injury	5 mm in diameter and 2 mm in depth	N/A	Yes	Day 14: largely regenerated
	Pig liver volumetric injury	10 mm in diameter and 10 mm in depth	N/A	Yes	Day 28: moderately regenerated
Surgicel[5]	Rat liver volumetric injury	5 mm in diameter and 2 mm in depth	N/A	Yes	Day 14: largely unregenerated
CoSeal[5]	Rat liver volumetric injury	5 mm in diameter and 2 mm in depth	N/A	Yes	Day 14: moderately regenerated
Liquid-infused microstructured bioadhesives[4]	Rat liver volumetric injury	4 mm in diameter and 3 mm in depth	Very mild	Yes	Day 14: largely unregenerated
Surgifoam[4]	Rat liver volumetric injury	4 mm in diameter and 3 mm in depth	Severe	Yes	Day 14: largely unregenerated
Microchannelled alkylated chitosan sponge[61]	Rat liver perforation injury	6 mm in diameter	N/A	N/A	Day 30: around 50% tissue ingrowth
Liver ECM-enriched gelatin sponge[62]	Rat liver incision	10 mm long and 5 mm thick	Mild	N/A	Day 14: largely unregenerated
Gelatin sponge[62]	Rat liver incision	10 mm long and 5 mm thick	Severe	N/A	Day 14: largely unregenerated
PEG bioadhesive[63]	Rat liver volumetric injury	10 mm in diameter and 2 mm in depth	Mild	N/A	Day 14: largely unregenerated Day 28: moderately regenerated
Cyanoacrylate adhesive[63]	Rat liver volumetric injury	10 mm in diameter and 2 mm in depth	Severe	N/A	Day 14: largely unregenerated Day 28: largely unregenerated
Surgicel[64]	Rat liver volumetric injury	5 mm in diameter and depth unreported	Severe	N/A	Day 14: largely unregenerated Day 28: largely unregenerated
Liver ECM loaded oxidized cellulose/chitosan composite[64]	Rat liver volumetric injury	5 mm in diameter and depth unreported	Mild	N/A	Day 14: moderately regenerated Day 28: largely regenerated

Notes: The liver regeneration profiles were estimated from the reported histology images.

Supplementary References:

56 Garyfallogiannis, K. et al. Fracture toughness of fibrin gels as a function of protein volume fraction: Mechanical origins. *Acta Biomater.* **159**, 49-62 (2023).

57 Baumberger, T. & Ronsin, O. From thermally activated to viscosity controlled fracture of biopolymer hydrogels. *J. Chem. Phys.* **130**, 061102 (2009).

58 Baumberger, T., Caroli, C. & Martina, D. Solvent control of crack dynamics in a reversible hydrogel. *Nat. Mater.* **5**, 552-555 (2006).

59 Ronsin, O., Naassaoui, I., Marcellan, A. & Baumberger, T. Environmental nanoparticle-induced toughening and pinning of a growing crack in a biopolymer hydrogel. *Phys. Rev. Lett.* **123**, 158002 (2019).

60 Liu, C. et al. Tough hydrogels with rapid self-reinforcement. *Science* **372**, 1078-1081 (2021).

61 Du, X. et al. Microchannelled alkylated chitosan sponge to treat noncompressible hemorrhages and facilitate wound healing. *Nat. Commun.* **12**, 4733 (2021).

62 Wang, B., Johnson, A. & Li, W. Development of an extracellular matrix-enriched gelatin sponge for liver wound dressing. *J. Biomed. Mater. Res. A* **108**, 2057-2068 (2020).

63 Huang, Y. et al. Highly Tough and Biodegradable Poly(ethylene glycol)-based bioadhesives for large-scaled liver injury hemostasis and tissue regeneration. *Adv. Healthcare Mater.*, e2301086 (2023).

64 Ibne Mahbub, M. S., Bae, S. H., Gwon, J. G. & Lee, B. T. Decellularized liver extracellular matrix and thrombin loaded biodegradable TOCN/Chitosan nanocomposite for hemostasis and wound healing in rat liver hemorrhage model. *Int. J. Biol. Macromol.* **225**, 1529-1542 (2023).